Cyclic superconducting refrigerators using guided fluxon propagation

Tathagata Karmakar,[1,2,3,*] Étienne Jussiau,[1,2,3,†] Sreenath K. Manikandan,[4,‡] and Andrew N. Jordan[3,1,2,§]
[1]*Department of Physics and Astronomy, University of Rochester, Rochester, New York 14627, USA*
[2]*Center for Coherence and Quantum Optics, University of Rochester, Rochester, New York 14627, USA*
[3]*Institute for Quantum Studies, Chapman University, Orange, California 92866, USA*
[4]*Nordita, KTH Royal Institute of Technology and Stockholm University, Hannes Alfvéns väg 12, SE-106 91 Stockholm, Sweden*

(Received 10 February 2023; revised 23 December 2023; accepted 3 January 2024; published 23 January 2024)

We propose cyclic refrigeration in solid state, employing a gas of magnetic field vortices in a type-II superconductor—also known as fluxons—as the cooling agent. Refrigeration cycles are realized by envisioning a racetrack geometry consisting of both adiabatic and isothermal arms, etched into a type-II superconductor. The guided propagation of fluxons in the racetrack is achieved by applying an external electrical current, in a Corbino geometry, through the sample. A gradient of magnetic field is set across the racetrack allowing one to adiabatically cool down and heat up the fluxons, which subsequently exchange heat with the cold and hot reservoirs, respectively. We characterize the steady state of refrigeration cycles thermodynamically for both *s*-wave and *d*-wave pairing symmetries, and present their figures of merit such as the cooling power delivered, and the coefficient of performance. Our cooling principle can offer significant cooling for on-chip microrefrigeration purposes, by locally cooling below the base temperatures achievable in a conventional dilution refrigerator. We estimate $\mathrm{nW/mm^2}$ of cooling power per unit area assuming a tunnel coupling with $\sim \mathrm{M\Omega\,\mu m^2}$ specific resistance. Integrating the fluxon fridge to quantum circuits can enhance their coherence time by locally suppressing thermal fluctuations, and improve the efficiency of single photon detectors and charge sensors.

DOI: 10.1103/PhysRevResearch.6.013085

I. INTRODUCTION

Quantum thermal machines have attracted increasing amounts of attention not only because of their fundamental importance in developing the field of quantum thermodynamics [1], but also because of the practical importance of controlling thermal transport in cryogenic environments [2]. Long-standing material science problems of low thermoelectric efficiencies can be overcome via energy-structured transport properties between coupled conductors [3]. In the field of mesoscopic physics, extensive research has been carried out to investigate thermoelectric devices [4], heat engines [5], thermometers [6], heat diodes [7], heat transistors [8], and refrigerators [9]. These devices are primarily focused on electrons as the charge and heat carriers based on quantum dots [10], quantum wells [11], quantum point contacts [12] and superlattices [13]. However, research focusing on other heat carriers including magnons [14], phonons [15], photons [16,17] has also advanced quickly. Not only a theoretical discipline but groundbreaking experiments have also been performed, realizing refrigerators [18] and heat engines leveraging the sharp energy transmission features of resonant tunneling quantum dots [19], current rectification properties of electron cavities coupled with quantum point contacts to Ohmic contacts [20,21], phonon assisted heat transport in double quantum dot [22], as well as driven superconductors to control heat currents [23,24]. Among additional experimental breakthroughs, nanoscale three-terminal energy harvester using coupled quantum dots [25], particle exchange heat engine exhibiting near thermodynamic efficiency [26], nonlocal thermoelectric current in a Cooper pair splitter comprised of graphene quantum dots connected across aluminum superconductor [27] have been realized. Together, these experiments have demonstrated high efficiency thermal machines operating on quantum principles.

Here, we consider another type of heat carrier, namely, a collection of fluxons treated thermodynamically. In a type-II superconductor, magnetic flux quanta can pierce the entropy-free Cooper-paired superconducting state, to produce an island of normal electrons in the core of each fluxon [28,29]. We utilize this fluxon as a bucket of entropy, shuttling it back and forth between hot and cold reservoirs. To make a thermodynamic cycle, our other control parameter is the local magnetic field [30–33]. By magnetizing or demagnetizing the fluxons, the small electron gas inside fluxon is cooled or heated. Therefore, the working substance is a fluxon gas which we treat at a thermodynamic level. When confined to a racetrack geometry, Fig. 1, the fluxon gas undergoes successive heating or cooling via the magnetic (de)magnetization from a gradient (out of plane) magnetic field, together with

*tkarmaka@ur.rochester.edu
†ejussiau@ur.rochester.edu
‡sreenath.k.manikandan@su.se
§jordan@chapman.edu

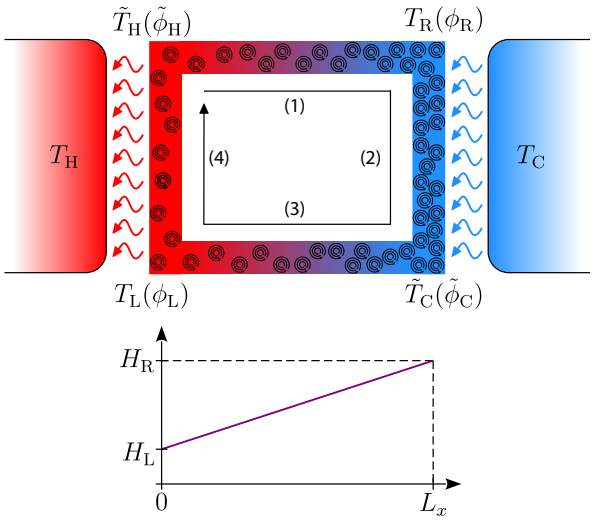

FIG. 1. Schematic of the type-II superconducting refrigerator geometry with two arms in contact with hot ($T_{\rm H}$) and cold ($T_{\rm C}$) reservoirs. A magnetic field (out of the page) gradient from arm (4) to arm (2) causes a gradient in the vortex density. An external current (not shown) flows outward in the Corbino geometry, driving the vortices along the arrow shown. The temperatures at the four corners represent the temperatures of the fluxons at the end of each stroke (see Secs. II and III). The values in the bracket represent the corresponding temperatures scaled with respect to that of the hot reservoir (see Sec. IV A). In subsequent analysis, we assume that the magnetic field varies linearly along the arm. The variation is shown in the plot below the schematic.

exposure to a hot or cold thermal reservoir. The remaining piece of the thermodynamic cycle is the motive force needed to drive the fluxons around the racetrack. This is provided by the Lorentz force [34,35], applied via a current bias applied in a Corbino geometry.

The thermal machine briefly described above may be used as a refrigerator to cool the cold reservoir. We focus on the physics of refrigeration using this concept of a cyclic superconducting refrigerator. Finding new cooling mechanisms at low temperature that do not rely on liquid helium-3, a precious resource, is an outstanding challenge to the low-temperature physics community. Principles of superconductivity offer another cooling paradigm, where the adiabatic magnetization of superconductors has been predicted to produce a cooling effect [36–38]. Efforts have been made to find realistic applications for this approach since the early days of superconductivity, especially using conventional (type-I) superconductors [39]. Recently, it has also been proposed that cyclic refrigerators can be conceptualized with type-I superconductors as the working substance, which can lead to practical quantum device implementations in solid state [40].

In contrast to type-I superconductors, the majority of nonelemental superconductors undergo a type-II phase transition into a mixed state with the magnetic field lines forming flux vortices [28,29], with each vortex, or fluxon, carrying a quantum ($h/2e$) of magnetic flux. These flux vortices are known to organize into characteristic lattice structures, known as Abrikosov lattices [28,41–43]. Individual fluxons have recently been proposed as information bits for efficient random-access memory devices [44]. Fluxons also interact with spin-waves in superconductor/ferromagnetic heterojunctions, suggesting opportunities for new avenues of hybrid electronic devices in the nanoscale [45]. On a related note, heat transport due to flux vortices in long Josephson junctions (also called Josephson vortices) has been studied [46–50]. The refrigerator proposed here further pushes the frontiers of fluxon based technologies to solid-state integrable quantum devices, which can offer substantial cooling below ambient base temperatures in cryogenic environments.

This article is organized as follows. Section II describes the refrigerator and provides an account of the relevant cycles. We also calculate the heat exchanged, the cooling power delivered, and the coefficient of performance for s-wave and d-wave superconductor based refrigerators. Section III provides a phenomenological description of fluxon propagation and heat exchange with the reservoirs for s-wave superconductors. In light of this description, we characterize the performance of the refrigerator in Sec. IV. Lastly, we discuss our findings in Sec. V and conclude in Sec. VI.

II. THE MODEL

We now expand on the description of our fluxon heat engine, described in the Introduction. An insightful analogy of this heat engine can be made to domestic refrigerators operating based on the principles of free expansion and compression of nonideal gases, cyclically moving through a cooling system. The fluxons moving through the Corbino racetrack geometry behave similarly, where the density of the "fluxon gas" in different regions is controlled by the local magnetic induction. Fluxons are colder in regions of high magnetic field as opposed to regions of lower magnetic field, owing to adiabatic conditions assumed. The effective description for a cooling cycle with adiabatic and isothermal arms is presented in greater detail in the subsequent sections, and is comparable to the well-known Otto cycles [51–53]. We consider fluxons in type-II superconductors of both s-wave and d-wave pairing symmetries, and provide a complete thermodynamic characterization, as well as discuss the laws of thermodynamics for the cyclic refrigerator.

A. Refrigeration cycle

We propose to design a magnetic Otto-type refrigerator with vortices in a type-II superconductor acting as the working substance. Vortices circulate between two heat reservoirs with temperatures $T_{\rm H} > T_{\rm C}$, extracting heat from the cold reservoir C (on the right in Fig. 1), and using the hot one H (on the left in Fig. 1) as a sink. In our analysis, vortex temperature refers to the quasiparticle temperature in the vortices. The refrigerator operates on a four-stroke cycle:

(1) Magnetization: Vortices at temperature $T_{\rm H}$ move from H to C along the upper arm of the racetrack through a positive magnetic field gradient. This leads to an increase in the fluxon density, and therefore increased density of states of the low energy quasiparticle excitations in the vortices [54]. This has the effect of cooling down the quasiparticles in the vortices to a temperature $T_{\rm R} < T_{\rm C}$.

(2) Heat extraction: The working substance at temperature T_R is put in contact with the cold reservoir C. Heat is extracted from the latter as the temperature of the working substance increases until it reaches the reservoir's value T_C. The magnetic field is kept at the constant value H_R throughout this step.

(3) Demagnetization: Vortices at temperature T_C move along the lower arm of the racetrack through a negative magnetic field gradient. The temperature of the working substance thus rises up to a value $T_L > T_H$.

(4) Heat rejection: The working substance at temperature T_L is put in contact with the hot reservoir H, in which it rejects heat until its temperature drops to T_H. The magnetic field is kept at the constant value H_L throughout this step.

Note that this description is purely macroscopic and thermodynamic. A microscopic description can also be interesting. However, such a description is beyond the scope of this article. In what follows, we assume the temperatures under consideration are much lower than the critical temperature of the superconductor. Additionally, the magnetic field is between the two critical values $H_{c1} < H < H_{c2}$, and close to H_{c1} so the intervortex interaction is negligible. Usually for type-II superconductors (cuprates or FeAs or Nb based for example), at $T = 0$, the first critical field $\mu_0 H_{c1}$ values are around $0.001 - 0.1$ T, while the second critical field $\mu_0 H_{c2}$ values can range between $10 - 100$ T [55]. For our refrigeration cycles, applied magnetic fields around $\mu_0 H \simeq 1$ T should be ideal experimentally. For superconductors with coherence lengths of the order of 1 nm, the intervortex distance $\xi\sqrt{H_{c2}/H}$ ~ 10 nm. Therefore, a sample of width $\sim$10 μm and $\sim$1 mm length will allow a macroscopic thermodynamic description of the vortices therein. We also assume that the magnetic field gradient and the speed at which vortices move across the racetrack are small enough such that magnetization and demagnetization strokes (1) and (3) are performed adiabatically.

B. *s*-wave model

We first consider the case of a conventional *s*-wave superconductor. A thermodynamic analysis of the engine cycle is possible given knowledge of the equation of state of the fluxons. In this situation, the main contribution to the specific heat comes from the vortex cores, each of them contributing a constant to the total specific heat, which is proportional to the vortex density as a result [54]. The specific heat [56], written as a function of the temperature T and the magnetic field H, then reads

$$C(T, H) = \gamma H T, \tag{1}$$

where γ is a constant. Given the definition $C(T, H) = T\,\partial S/\partial T|_H$, we can take the entropy to be

$$S(T, H) = \gamma H T. \tag{2}$$

To obtain the amount of heat extracted from the cold reservoir and the work that must be exerted on the working substance to power the refrigerator, one must calculate the variations of the working substance's internal energy throughout each stroke of the cycle. We consequently introduce the internal energy U through its differential, which is naturally expressed in terms of the entropy S and the magnetization M [55],

$$dU = T\,dS + \mu_0 H\,dM, \tag{3}$$

where μ_0 denotes the vacuum permeability. However, the pair of variables adapted to our cycle consists of the entropy S and the magnetic field H since strokes (1) and (3) take place at constant entropy and strokes (2) and (4) take place at constant magnetic field. We obtain an expression for the energy differential in terms of S and H by expanding dM in Eq. (3) above,

$$dU = \left(T + \mu_0 H \left.\frac{\partial M}{\partial S}\right|_H\right) dS + \mu_0 H \left.\frac{\partial M}{\partial H}\right|_S dH. \tag{4}$$

We can obtain an expression for the partial derivative of the magnetization with respect to the entropy using a Maxwell relation [55]. We consider the magnetic enthalpy $K = U - \mu_0 HM$ whose differential is given by

$$dK = T\,dS - \mu_0 M\,dH. \tag{5}$$

Invoking the symmetry of second derivatives, we find

$$\left.\frac{\partial M}{\partial S}\right|_H = -\frac{1}{\mu_0}\left.\frac{\partial T}{\partial H}\right|_S = \frac{S}{\mu_0 \gamma H^2}, \tag{6}$$

where we have used the explicit expression for the entropy from Eq. (2). Integrating Eq. (6) above over the entropy then yields

$$M(S, H) = \frac{S^2}{2\mu_0 \gamma H^2} + A_s(H), \tag{7}$$

where $A_s(H)$ denotes the integration "constant" for the integration over S and is thus a function of H only. Physically, it corresponds to the magnetization at zero entropy, $A_s(H) = M(S = 0, H)$. Since M and H are thermodynamically conjugate variables, it is not possible to find an explicit expression for $A_s(H)$ using Maxwell relations; it can only be derived from a microscopic model. The energy differential in Eq. (4) can eventually be rewritten as

$$dU = \frac{2S}{\gamma H}\,dS - \left(\frac{S^2}{\gamma H^2} - \mu_0 H \frac{dA_s}{dH}\right) dH. \tag{8}$$

The energy changes during strokes (1) and (3) correspond to the magnetic work done on the superconductor in order to fuel the refrigeration process. We assume that these magnetization and demagnetization steps are performed adiabatically. Hence, $S = S_1 = \gamma H_L T_H$ throughout stroke (1) and $S = S_3 = \gamma H_R T_C$ throughout stroke (3). We then derive the magnetic work,

$$\begin{aligned} W &= \int_{(1)} dU|_{S=S_1} + \int_{(3)} dU|_{S=S_3} \\ &= -\frac{S_1^2 - S_3^2}{\gamma} \int_{H_L}^{H_R} \frac{dH}{H^2} \\ &= \gamma (H_R - H_L)\left(\frac{H_R}{H_L} T_C^2 - \frac{H_L}{H_R} T_H^2\right). \end{aligned} \tag{9}$$

Further, the temperature of the working substance throughout strokes (1) and (3) can be easily calculated using the fact

that the entropy remains constant. In particular, the temperatures T_R and T_L at the end of strokes (1) and (3) respectively are given by

$$T_R = \frac{S_1}{\gamma H_R} = \frac{H_L}{H_R} T_H, \tag{10}$$

$$T_L = \frac{S_3}{\gamma H_L} = \frac{H_R}{H_L} T_C. \tag{11}$$

During stroke (2), the magnetic field stays constant, $H = H_R$, while the entropy varies from S_1 to S_3. The energy variation during this step corresponds to the heat extracted from the cold reservoir,

$$Q_C = \int_{(2)} dU|_{H=H_R} = \frac{2}{\gamma H_R} \int_{S_1}^{S_3} S\, dS = \gamma H_R \left(T_C^2 - \frac{H_L^2}{H_R^2} T_H^2 \right). \tag{12}$$

Refrigeration takes place when heat is extracted from the cold reservoir, that is $Q_C \geqslant 0$. We see in Eq. (13) that this imposes

$$\frac{H_L}{H_R} \leqslant \frac{T_C}{T_H}. \tag{13}$$

We also note that $W \geqslant 0$ when the condition in Eq. (13) is satisfied.

The heat rejected in the hot reservoir during stroke (4) can be calculated in a similar manner: During this step, the magnetic field is constant during stroke (4), $H = H_L$, while the entropy goes from S_3 to S_1. We then find that

$$Q_H = \int_{(4)} dU|_{H=H_L} = \gamma H_L \left(T_H^2 - \frac{H_R^2}{H_L^2} T_C^2 \right). \tag{14}$$

We immediately see that $Q_H < 0$ when the condition in Eq. (13) is satisfied. Further, it is straightforward to check that $W + Q_C + Q_H = 0$, which corresponds to the first law of thermodynamics: The variation of internal energy during a cycle is zero. As for the second law of thermodynamics, it can be expressed via the Clausius inequality [57],

$$\frac{Q_C}{T_C} + \frac{Q_H}{T_H} \leqslant 0. \tag{15}$$

One can check that the expressions for Q_C and Q_H in Eqs. (13) and (14) respectively satisfy Eq. (15) above.

The refrigerator's coefficient of performance (COP) is given by the ratio of the heat extracted from the cold reservoir to the work supplied to the superconductor,

$$\mathrm{COP} = \frac{\mathrm{Q_C}}{\mathrm{W}} = \frac{\mathrm{H_L}}{\mathrm{H_R} - \mathrm{H_L}} = \frac{\mu}{1-\mu}, \tag{16}$$

similar to Otto cycle results, where $\mu = H_L/H_R$. Using the first and second laws of thermodynamics, one can show that the refrigerator's COP is upper bounded by the Carnot COP, which is reached when the refrigerator operates reversibly,

$$\mathrm{COP} = \frac{\mu}{1-\mu} \leqslant \mathrm{COP_{Carnot}} = \frac{\mathrm{T_C}}{\mathrm{T_H} - \mathrm{T_C}}. \tag{17}$$

Carnot's theorem in Eq. (17) is equivalent to Eq. (13) in the situation at stake. We then find that Carnot COP is reached when $\mu = T_C/T_H$, in which case $Q_C = 0$.

C. *d*-wave model

In the case of a d-wave superconductor, the specific heat calculated using the Volovik model is given by [54,58]

$$C(T, H) = \alpha \sqrt{H} T, \tag{18}$$

where α is again a constant. Applying the same treatment as in the case of an s-wave superconductor, we first calculate the entropy,

$$S = \alpha \sqrt{H} T. \tag{19}$$

We can now obtain a formal expression for the magnetization. We have

$$\left.\frac{\partial M}{\partial S}\right|_H = -\frac{1}{\mu_0} \left.\frac{\partial T}{\partial H}\right|_S = \frac{S}{2\mu_0 \alpha H^{3/2}}, \tag{20}$$

which leads to

$$M(S, H) = \frac{S^2}{4\mu_0 \alpha H^{3/2}} + A_d(H), \tag{21}$$

where $A_d(H) = M(S = 0, H)$ is an unknown function of the magnetic field. As a consequence, the differential for the internal energy expressed in the relevant variables S and H is given by

$$dU = \frac{3S}{2\alpha\sqrt{H}}\, dS - \left(\frac{3S^2}{8\alpha H^{3/2}} - \mu_0 H \frac{dA_d}{dH} \right) dH. \tag{22}$$

The temperatures at the end of strokes (1) and (3) can be again obtained using the constant entropy condition,

$$T_R^{\mathrm{d}} = \sqrt{\frac{H_L}{H_R}}\, T_H, \tag{23}$$

$$T_L^{\mathrm{d}} = \sqrt{\frac{H_R}{H_L}}\, T_C, \tag{24}$$

where we include superscript d to distinguish the temperatures from Eqs. (10) and (11). The entropies during these two strokes are $S_1^{\mathrm{d}} = \alpha\sqrt{H_L} T_H$ and $S_3^{\mathrm{d}} = \alpha\sqrt{H_R} T_C$. The work supplied to the superconductor during a cycle is then calculated as in Eq. (10), and we obtain

$$W = \frac{3\alpha}{4} \left(\sqrt{H_R} - \sqrt{H_L} \right) \left(\sqrt{\frac{H_R}{H_L}} T_C^2 - \sqrt{\frac{H_L}{H_R}} T_H^2 \right). \tag{25}$$

Conversely, strokes (2) and (4) take place at constant magnetic fields, and we calculate Q_C and Q_H as in Eqs. (13) and (14) respectively to find

$$Q_C = \frac{3\alpha\sqrt{H_R}}{4} \left(T_C^2 - \frac{H_L}{H_R} T_H^2 \right), \tag{26}$$

$$Q_H = \frac{3\alpha\sqrt{H_L}}{4} \left(T_H^2 - \frac{H_R}{H_L} T_C^2 \right). \tag{27}$$

It is clear from Eq. (26) that refrigeration is only possible when

$$\frac{H_L}{H_R} \leqslant \frac{T_C^2}{T_H^2}, \tag{28}$$

in which case $Q_C \geqslant 0$, $Q_H \leqslant 0$ and $W \geqslant 0$.

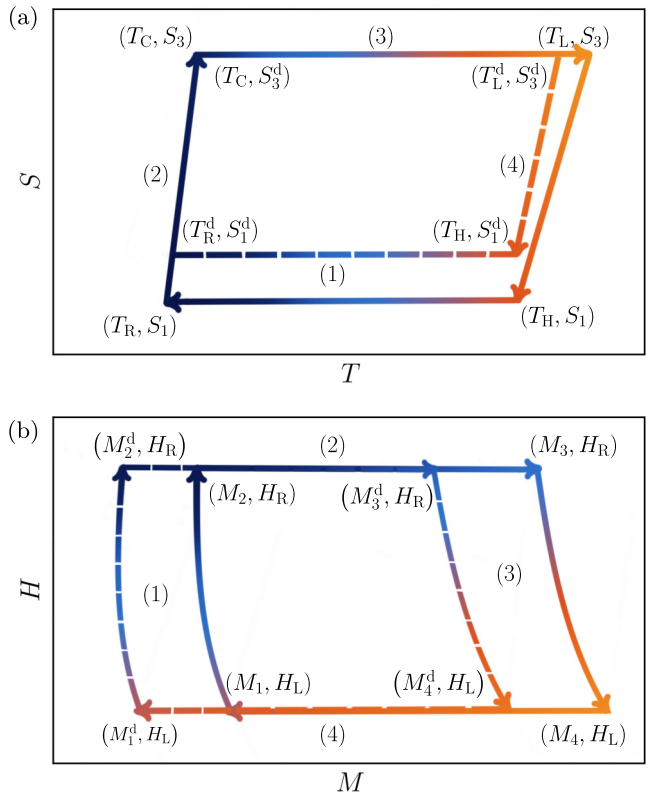

FIG. 2. These illustrations show the qualitative thermodynamic behavior of the fluxons as they move along the racetrack. Panel (a) shows the fluxons in ST plane as they complete a full cycle for both s-wave (solid) and d-wave (dashed) superconductors. The temperatures and entropies at the end of each stroke are mentioned. For this illustration, we assume that γ in Eq. (2) and α in Eq. (19) have values such that the fluxons have same entropy after they are in contact with the cold bath [after stroke (2)], i.e., $S_3 = S_3^d$. The cycle in ST plane for both types of superconductors are trapezoids in shape. The slope of arms representing strokes (2) and (4) are proportional to the corresponding magnetic field. Therefore, the slope is smaller in magnitude for stroke (4). Panel (b) shows the behavior of the fluxons in HM plane. We assume $A_s(H) = A_d(H) = 0$ for the illustration. Here, $M_1 = \frac{\gamma}{2\mu_0} T_H^2, M_2 = \frac{\gamma}{2\mu_0} T_R^2, M_3 = \frac{\gamma}{2\mu_0} T_C^2$ and $M_4 = \frac{\gamma}{2\mu_0} T_L^2$. Similarly, $M_1^d = \frac{\alpha}{4\mu_0} \frac{T_H^2}{\sqrt{H_L}}, M_2^d = \frac{\alpha}{4\mu_0} \frac{(T_R^d)^2}{\sqrt{H_R}}, M_3^d = \frac{\alpha}{4\mu_0} \frac{T_C^2}{\sqrt{H_R}}$, and $M_4^d = \frac{\alpha}{4\mu_0} \frac{(T_L^d)^2}{\sqrt{H_L}}$. Strokes (1) and (3) express the nonlinear dependence of the magnetization M on H. The area inside the loops represent the work done by the refrigerator.

Finally, the refrigerator's COP is given by

$$\mathrm{COP} = \frac{Q_C}{W} = \frac{\sqrt{H_L}}{\sqrt{H_R} - \sqrt{H_L}} = \frac{\sqrt{\mu}}{1 - \sqrt{\mu}}. \tag{29}$$

Similarly to the case of an s-wave superconductor, the refrigeration condition in Eq. (28) is equivalent to $\mathrm{COP} \leqslant \mathrm{COP}_{\mathrm{Carnot}}$. The Carnot coefficient of performance is achieved when equality is realized in Eq. (28), in which case $Q_C = 0$.

In Fig. 2 we show the fluxons in ST and HM planes as they complete the refrigeration cycles for both s-wave and d-wave superconductors. The thermodynamic cycle in ST plane is trapezoidal. In the HM plane they are represented by the enclosed region of two parallel lines and two smooth nonlinear curves.

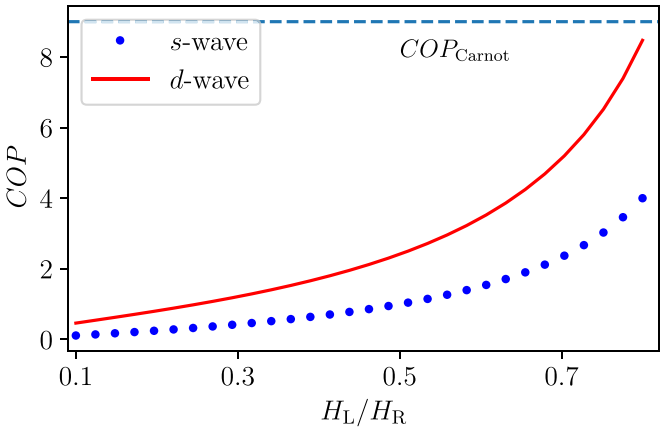

FIG. 3. Plot of the fluxon refrigerator COP as a function of the ratio of the magnetic fields on the left and right arms. The blue dots (red line) shows the COP for an s-wave (d-wave) superconductor. We see that as the magnetic fields come closer to one another, the COP increases. Also, the COP for a d-wave superconductor is higher than that of an s-wave superconductor under the same conditions. For both s and d-wave cases, the reservoir temperatures set the maximum possible value of the magnetic field ratio [see Eqs. (13) and (28)]. The dashed horizontal line corresponds to $\mathrm{COP}_{\mathrm{Carnot}}$ when $T_C/T_H = 0.9$.

D. Results

From Eqs. (16) and (29), it is clear that the coefficient of performance only depends on the applied magnetic fields for both s-wave and d-wave superconductors. Figure 3 shows the behavior of the coefficient of performance for both of these cases as functions of the magnetic field ratio H_L/H_R. The COP clearly increases with this ratio and reaches its maximal value when the refrigerator operates reversibly, in which case no refrigeration occurs. This is achieved when $H_L/H_R = T_C/T_H$ for s-wave superconductors and $H_L/H_R = T_C^2/T_H^2$ for d-wave superconductors. Additionally, both kinds of superconductors exhibit similar behaviors, although d-wave superconductors show slightly better performance. For simplicity, we focus on s-wave superconductors throughout the rest of our analysis. Analogous explorations can be considered for d-wave superconductors and are expected to lead to similar qualitative conclusions.

III. FLUXON PROPAGATION AND DISSIPATION

In reality, this simple model above needs to be augmented to take into account the energy loss of the fluxons as they are being driven around the racetrack, and the effects of vortex thermalization at finite velocities.

A. Propagation of fluxons in the steady state

Taking a mesoscopic sample of the fluxon lattice as the working substance, we first consider the following simple form for the heat capacity per unit volume for s-wave superconductors $C(T, H) = \gamma HT$. The entropy is $S(T, H) = \gamma HT$.

Given that entropy $S(T, H)$ is a state function, it can be written as an exact differential of the form,

$$\frac{dS}{dx} = \frac{\partial S}{\partial T}\frac{dT}{dx} + \frac{\partial S}{\partial H}\frac{dH}{dx} = \gamma(H\partial_x T + T\partial_x H), \tag{30}$$

where x is the length along the arms.

Recall that adiabatic processes are processes where the system is supposed to be thermally isolated from the environment. Heat losses can be taken to account by modifying $\frac{dS}{dx} = 0$ to $\frac{dS}{dx} = \frac{1}{v}\frac{P(x)}{T(x)}$, where $P(x)$ is the power loss due to dissipation along an arm and v is the speed of fluxons (also see Appendix). The differential equations modify to

$$\frac{P(x)}{T(x)} = \gamma v(H(x)\partial_x T(x) + T(x)\partial_x H(x)). \tag{31}$$

This can be solved for different adiabatic and isothermal arms of the cycle, accounting for additional dissipation mechanisms in $P(x)$.

B. Incorporating dissipation

In steady state, the damping coefficient η results in an opposing force $f = -\eta v$. The driving force from the current is given by

$$\vec{F} = \vec{J} \times \phi_0 \hat{u}, \tag{32}$$

where the unit vector $\hat{u}$ is parallel to the vortex, and the electrical current $\vec{J}$ is arranged to flow from the inner edge to the outer edge of the sample. $\phi_0 = \frac{h}{2e}$ is the magnetic flux quantum. In the steady state, the dissipative force cancels the Lorentz-like force, resulting in the steady-state velocity of $v = J\phi_0/\eta$. We can utilize the discussion in the previous section to incorporate the effect of dissipation in our description. In this case $P(x) = n(x)\eta v^2$, where $n(x)$ is the surface density of fluxons at position x [55,59]. Therefore, for step (1) we have (in the steady state),

$$\frac{\partial S}{\partial x} = \frac{n(x)\eta v}{T(x)}. \tag{33}$$

Next, we assume $n(x) = n_{\mathrm{L}}(1 + \frac{x}{L_x}(1/\mu - 1))$, where n_L is the fluxon density in the arm in contact with the hot reservoir and L_x is the length of the arms along which there is a magnetic field gradient [i.e., arms (1) and (3)]. In other words, assuming linearly varying magnetic field, and using expression (2), for s-wave superconductors we get

$$T_{\mathrm{R}} = \left(\mu^2 \tilde{T}_H^2 + \frac{2\mu_0 J L_x}{3\gamma}(1 + \mu + \mu^2)\right)^{1/2}. \tag{34}$$

Here $\tilde{T}_{\mathrm{H}}$ is the final temperature of the fluxons after step (4), and could be different from T_{H} due to dissipation (as we will see soon). Similarly, after step (3)

$$T_{\mathrm{L}} = \left(\frac{\tilde{T}_C^2}{\mu^2} + \frac{2\mu_0 J L_x}{3\gamma\mu^2}(1 + \mu + \mu^2)\right)^{1/2}, \tag{35}$$

where $\tilde{T}_{\mathrm{C}}$ is the final temperature of fluxons after stroke (2). Without dissipation, Eqs. (34) and (35) reduce to Eqs. (10) and (11), as expected.

C. Simple dynamical model for heat exchanges

In this section, we introduce a simple model to analyze the dynamics of the heat exchanges between the reservoirs and the working substance as the latter moves along the superconductor geometry. At the beginning of stroke (2), $y = 0$, its temperature is T_{R}, and it is coupled to the cold reservoir at temperature $T_{\mathrm{C}} > T_{\mathrm{R}}$.

The working substance moves at a constant speed v and spends a time L_y/v in contact with the reservoir, where L_y is the length of the racetrack in the relevant direction. The magnetic field does not change during this process, $H = H_{\mathrm{R}}$. As the working substance moves along the track, it receives heat from the reservoir and dissipates energy due to vortex drag. In time dt, the working substance moves a distance $dy = vdt$ along the track. During this infinitesimal distance traveled, both the heat exchange with the reservoir and the heat generated due to electrical current contributes to the change in the fluxons' internal energy. The energy balance (per unit volume) in interval dy along the racetrack reads

$$U(y + dy) - U(y) = (\dot{Q} + n_{\mathrm{R}}\eta v^2)\frac{dy}{v}, \tag{36}$$

where $U(y)$ is the energy density of the working substance at position y, $\dot{Q}$ is the heat current per unit volume from the reservoir, and n_{R} is the vortex density on the right arm. The second term to the right-hand side above corresponds to the energy transferred to the working substance so that the vortex speed v remains constant despite the drag force. This is done practically by imposing an electrical current flow in the direction perpendicular to the vortex motion.

We introduce a phenomenological Fourier-type formula for the heat current $\dot{Q}$,

$$\dot{Q} = -\kappa_{\mathrm{th}}(T - T_{\mathrm{C}}), \tag{37}$$

where T is the temperature of the working substance, and κ_{th} denotes the thermal conductivity (per unit volume) at the contact with the reservoir. The thermal conductivity is assumed to be temperature and position independent for simplicity (see Sec. IV B). The expression for the heat current in Eq. (37) is naturally valid when the temperature difference $T - T_{\mathrm{C}}$ is small, but it often holds outside this regime.

Finally, we choose temperature and magnetic field as the relevant variables to describe the state of the working substance. As a consequence, the energy density is expressed through these quantities,

$$U(y) = U(T(y), H(y)) = U(T(y), H_{\mathrm{R}}). \tag{38}$$

We can now rewrite the energy time derivative as

$$\frac{dU}{dy} = \frac{dT}{dy}\frac{\partial U}{\partial T}\bigg|_H = \left(T\frac{\partial S}{\partial T}\bigg|_H + \mu_0 H\frac{\partial M}{\partial T}\bigg|_H\right)\frac{dT}{dy} = 2\gamma H T\frac{dT}{dy}, \tag{39}$$

where $\partial M/\partial T|_H$ has been calculated using the same technique that yielded Eq. (6). The energy balance in Eq. (36) then becomes

$$2v\gamma H_{\mathrm{R}} T\frac{dT}{dy} = -\kappa_{\mathrm{th}}(T - T_{\mathrm{C}}) + n_{\mathrm{R}}\eta v^2. \tag{40}$$

As a consequence, the temperature of the working substance obeys the following differential equation:

$$\frac{dT}{dy} = \frac{\kappa_{\rm th} T_{\rm C} + n_{\rm R}\eta v^2}{2v\gamma H_{\rm R} T} - \frac{\kappa_{\rm th}}{2v\gamma H_{\rm R}}. \tag{41}$$

The differential equation above can be solved analytically, and we find that the temperature reads

$$T(y) = T_{\rm fR}\left(1 + W\left(\left(\frac{T_{\rm R}}{T_{\rm fR}} - 1\right)e^{\frac{T_{\rm R}}{T_{\rm fR}} - 1 - y/v\tau_{\rm R}}\right)\right), \tag{42}$$

where W denotes the Lambert function, while the constants $\tilde{T}_{\rm fR}$ and $\tau_{\rm R}$ are given by

$$T_{\rm fR} = T_{\rm C} + \frac{n_{\rm R}\eta v^2}{\kappa_{\rm th}}, \quad \tau_{\rm R} = \frac{2\gamma H_{\rm R} T_{\rm fR}}{\kappa_{\rm th}}. \tag{43}$$

$T_{\rm fR}$ is the final temperature reached by the working substance if it were to stay in contact with reservoir C for an infinitely long time, and $\tau_{\rm R}$ is the characteristic time over which the working substance reaches its final temperature.

We observe that the asymptotic final temperature of the working substance $T_{\rm fR}$ is higher than $T_{\rm C}$ when dissipation is taken into account. As a result, the heat current $\dot{Q}$ starts to flow from the working substance to the reservoir after some time to the detriment of refrigeration. When the working substance travels slowly across the racetrack, the final temperature approaches the reservoir temperature,

$$T_{\rm fR} \simeq T_{\rm C} \quad \text{if} \quad v \ll \sqrt{\frac{\kappa_{\rm th} T_{\rm C}}{n_{\rm R}\eta}}. \tag{44}$$

The total heat exchanged with the cold reservoir is given by

$$Q_{\rm C} = \int_0^{L_y} dy\, \dot{Q}/v = -\tfrac{\kappa_{\rm th}}{v}\int_0^{L_y} dy\,(T(y) - T_{\rm C}). \tag{45}$$

The integration can be carried out analytically, and we find

$$Q_{\rm C} = \frac{\kappa_{\rm th} L_y}{v}(T_{\rm C} - T_{\rm fR}) - \frac{\kappa_{\rm th}\tau_{\rm R} T_{\rm fR}}{2}\left(\frac{T_{\rm R}}{T_{\rm fR}}\right)^2 + \frac{\kappa_{\rm th}\tau_{\rm R} T_{\rm fR}}{2}\left(1 + W\left(\left(\frac{T_{\rm R}}{T_{\rm fR}} - 1\right)e^{\frac{T_{\rm R}}{T_{\rm fR}} - 1 - L_y/v\tau_{\rm R}}\right)\right)^2. \tag{46}$$

In a similar manner, stroke (4) leads to cooling of the working substance from $T_{\rm L}$ to a final temperature $T_{\rm fL}$. In this case, Eq. (40) takes the form (assuming the same thermal conductivity)

$$\frac{dU}{dy} = \frac{dT}{dy}\frac{\partial U}{\partial T}\bigg|_H$$
$$\Rightarrow 2v\gamma H_{\rm L} T\frac{dT}{dy} = -\kappa_{\rm th}(T - T_{\rm H}) + n_{\rm L}\eta v^2. \tag{47}$$

Therefore,

$$T(y) = T_{\rm fL}\left(1 + W\left(\left(\frac{T_{\rm L}}{T_{\rm fL}} - 1\right)e^{\frac{T_{\rm L}}{T_{\rm fL}} - 1 - y/v\tau_{\rm L}}\right)\right), \tag{48}$$

where the constants $T_{\rm fL}$ and $\tau_{\rm L}$ are given by

$$T_{\rm fL} = T_{\rm H} + \frac{n_{\rm L}\eta v^2}{\kappa_{\rm th}}, \quad \tau_{\rm L} = \frac{2\gamma H_{\rm L} T_{\rm fL}}{\kappa_{\rm th}}. \tag{49}$$

Heat transferred to the hot reservoir is given by

$$Q_{\rm H} = \frac{\kappa_{\rm th} L_y}{v}(T_{\rm fL} - T_{\rm H}) + \frac{\kappa_{\rm th}\tau_{\rm L} T_{\rm fL}}{2}\left(\frac{T_{\rm L}}{T_{\rm fL}}\right)^2 - \frac{\kappa_{\rm th}\tau_{\rm L} T_{\rm fL}}{2}\left(1 + W\left(\left(\frac{T_{\rm L}}{T_{\rm fL}} - 1\right)e^{\theta_{\rm L} - 1 - L_y/v\tau_{\rm L}}\right)\right)^2. \tag{50}$$

IV. QUANTITATIVE ANALYSIS OF THE HEAT EXCHANGED AND REFRIGERATOR PERFORMANCE

With all the necessary physics at hand, we now analyze how the fluxon dynamics influence the heat exchanged and the refrigerator's performance.

A. Refrigeration cycle description in terms of dimensionless control parameters

We can analyze the system's behavior by looking at five independent dimensionless parameters

$$l = L_y/L_x, \quad \mu = H_{\rm L}/H_{\rm R}, \quad \phi_{\rm C} = T_{\rm C}/T_{\rm H},$$
$$\bar{v} = v\frac{2\gamma H_{\rm R} T_{\rm H}}{\kappa_{\rm th} L_x}, \quad \Omega = \frac{\mu_0\kappa_{\rm th}\eta L_x^2}{2\phi_0\gamma^2 H_{\rm R} T_{\rm H}^3}. \tag{51}$$

Here l signifies the geometry of the superconducting material. μ and $\phi_{\rm C}$ are the magnetic field ratio and reservoir temperatures ratio respectively. $\bar{v}$ is the dimensionless speed of the fluxons. Ω is a parameter signifying dissipation and depends on superconductor properties, length along x, magnetic field on the right-hand side, and hot reservoir temperature. We also define temperatures scaled with respect to the hot reservoir temperature as $\phi = T/T_{\rm H}$. The temperatures at the end of stroke (2) and (4) are

$$\tilde{\phi}_{\rm C} = \phi_{\rm fR}\left(1 + W\left(\left(\frac{\phi_{\rm R}}{\phi_{\rm fR}} - 1\right)e^{\frac{\phi_{\rm R}}{\phi_{\rm fR}} - 1 - \frac{l}{\bar{v}\phi_{\rm fR}}}\right)\right),$$
$$\tilde{\phi}_{\rm H} = \phi_{\rm fL}\left(1 + W\left(\left(\frac{\phi_{\rm L}}{\phi_{\rm fL}} - 1\right)e^{\frac{\phi_{\rm L}}{\phi_{\rm fL}} - 1 - \frac{l}{\mu\bar{v}\phi_{\rm fL}}}\right)\right), \tag{52}$$

with $\phi_{\rm fR} = \phi_{\rm C} + \frac{1}{2}\bar{v}^2\Omega$ and $\phi_{\rm fL} = 1 + \frac{1}{2}\bar{v}^2\mu\Omega$. Also, Eqs. (34) and (35) become

$$\phi_{\rm R}^2 = \mu^2\tilde{\phi}_{\rm H}^2 + \frac{2\bar{v}\Omega}{3}(1 + \mu + \mu^2),$$
$$\phi_{\rm L}^2 = \frac{\tilde{\phi}_{\rm C}^2}{\mu^2} + \frac{2\bar{v}\Omega}{3\mu^2}(1 + \mu + \mu^2). \tag{53}$$

Figure 4 shows the behavior of the fluxon temperatures in strokes 2 and 4 as functions of the distance traveled. At the end of the stroke, they tend to the temperatures of corresponding reservoirs.

The heat extracted from the cold reservoir is

$$Q_{\rm C} = \gamma H_{\rm R} T_{\rm H}^2\left(-l\bar{v}\Omega + \left(\tilde{\phi}_{\rm C}^2 - \phi_{\rm R}^2\right)\right). \tag{54}$$

When the speed $\bar{v}$ is slow enough, the exponential factor inside the Lambert function is negligible as compared with any integer power of $\bar{v}$. This allows us to neglect the Lambert function in Eq. (52) to obtain $\tilde{\phi}_{\rm C} \simeq \phi_{\rm fR}$ and

$$Q_{\rm C} \simeq \gamma H_{\rm R} T_{\rm H}^2\left(-l\bar{v}\Omega + \left(\phi_{\rm fR}^2 - \phi_{\rm R}^2\right)\right) \quad \text{if} \quad \bar{v} \ll \frac{l}{\phi_C}. \tag{55}$$

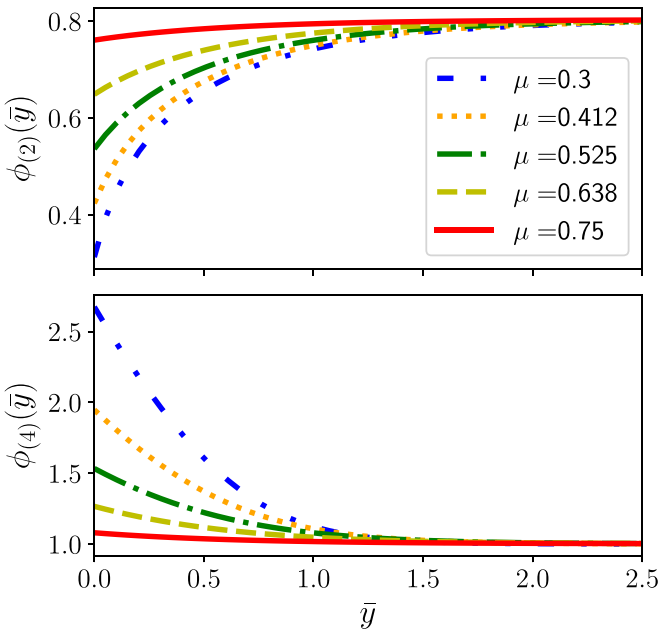

FIG. 4. Temperature as a function of scaled length $\bar{y} = y/L_x$ along the arms in contact with reservoirs in stroke 2 (top) and 4 (bottom) for different values of the magnetic field ratio. Here we have chosen $\phi_C = 0.8$, $l = 2.5$, $\bar{v} = 0.8$, $\Omega = 0.01$. We see that the temperature in stroke 2 (4) increases (decreases) and tends to a value close to ϕ_C ($\phi_H = 1$). With the decrease of the magnetic field, the initial temperature decreases (increases) in the top (bottom) plot. This behavior can be understood from Eqs. (10) and (11), where the temperature at the end of stroke 1 (3) is proportional (inversely proportional) to the magnetic field ratio.

The condition $\bar{v} \ll \frac{l}{\phi_C}$ provides a lower bound on the arm length ratio needed to ensure sufficient time for the fluxons to exchange heat with the cold reservoir. Using the approximate expression in Eq. (55), one can check that Q_C decreases with $\bar{v}$ at slow speeds. This behavior is well captured by a first-order expansion in v, which amounts to neglecting the difference between ϕ_{fR} and ϕ_C following the criterion in Eq. (44) (or equivalently $\bar{v} \ll \sqrt{1/\Omega}$). We then have

$$Q_C \simeq \gamma H_R T_H^2 \left(\left(\phi_C^2 - \mu^2\right) - \Omega\left(l + \tfrac{2}{3}\left(1 + \mu + \mu^2\right)\right)\bar{v}\right). \quad (56)$$

This decrease of Q_C with $\bar{v}$ indicates that the refrigerator can only operate at slow speeds. Indeed, Q_C becomes negative when $\bar{v}$ exceeds the speed limit $\bar{v}_{\mathrm{lim},R}$ given by

$$\bar{v}_{\mathrm{lim},R} = \frac{\phi_C^2 - \mu^2}{\Omega\left(l + \frac{2}{3}(1 + \mu + \mu^2)\right)}. \quad (57)$$

Numerical results using the analytical expression for Q_C in Eq. (54) confirm that refrigeration is only possible at slow speeds, with $\bar{v}_{\mathrm{lim},R}$ in Eq. (57) being a good estimate for the exact speed limit. Furthermore, the approximate expression for Q_C in Eq. (56) shows that the maximum amount of heat extracted from the cold reservoir is reached for $\bar{v} \to 0$. We then find

$$Q_C^{\max} = \gamma H_R T_H^2 \left(\phi_C^2 - \mu^2\right), \quad (58)$$

which is the result in Eq. (13). Thus, for refrigeration to occur, we must have $\phi_C \geqslant \mu$, see Eq. (13).

Our dynamical model also allows for the calculation of the refrigerator's cooling power. The latter is given by the ratio of the heat extracted from the cold reservoir to the time necessary to perform such extraction,

$$P_C = \frac{Q_C}{L_y/v} = \frac{\kappa_{th} T_H}{2} \frac{\bar{v}}{l}\left(-l\bar{v}\Omega + \left(\tilde{\phi}_C^2 - \phi_R^2\right)\right). \quad (59)$$

We can use Eq. (56) to approximate

$$P_C \simeq \frac{\kappa_{th} T_H}{2} \frac{\bar{v}}{l}\left(\left(\phi_C^2 - \mu^2\right) - \Omega\left(l + \frac{2}{3}(1 + \mu + \mu^2)\right)\bar{v}\right). \quad (60)$$

We then find that the cooling power reaches its maximum value for $\bar{v} = \bar{v}_{\mathrm{lim},R}/2$, and we have

$$P_C^{\max} \simeq \frac{\kappa_{th} T_H}{2} \frac{\left(\phi_C^2 - \mu^2\right)^2}{4l\Omega\left(l + \frac{2}{3}(1 + \mu + \mu^2)\right)}. \quad (61)$$

It is noteworthy that Eqs. (52) and (54) are implicit in nature, and could be solved numerically for arbitrary parameter values.

In Fig. 5, we show the cooling power and the heat withdrawn from the cold reservoir as functions of fluxon speed for different values of the magnetic field ratios. The cooling power has a parabola-like shape as a function of velocity, while the heat exchanged decreases almost linearly. Such parabolic dependence of cooling power on the velocity is typical in linear response theory. Similar dependence is observed for power generated in thermoelectric devices as a function of voltage. The approximations in Eqs. (56), (60), and (61) describe the behavior of the heat withdrawn and cooling power really well for larger values of the magnetic field ratio, till the point where refrigeration is no longer possible.

B. Experimentally realizable values of the cooling power and fluxon speed

To provide an estimate of the achievable cooling power, we assume that the cold reservoir is a normal metal, connected to the superconducting material through a thin insulating barrier, thus realizing a tunnel junction [60]. The heat transfer to the magnetic field vortices occurs through quasiparticle tunneling through the junction. Assuming the area of contact to be A and the width of the racetrack circulating fluxons to be w, the energy transported via the quasiparticles per unit time is [40,61]

$$P^{qp} = \frac{2A}{e^2 \mathcal{R}_s} \int_0^\infty dE\, E\left(f_{FD}(T_C) - f_{FD}(T)\right). \quad (62)$$

Here, f_{FD} refers to the Fermi-Dirac distribution and $\mathcal{R}_s$ is the specific resistance of the junction. A microscopic description will require incorporation of junction properties as well as energy barrier experienced by quasiparticles going in and out of the surface [63]. Based on phenomenology, the junction can be understood as an NSIN junction, including a thin superconducting layer that separates flux vortices from the interface. Such junction can be modeled as a NIN junction with exponentially suppressed transition amplitude. Also, in general the rate of energy transport depends on the position of contact since fluxons away from the contact will experience

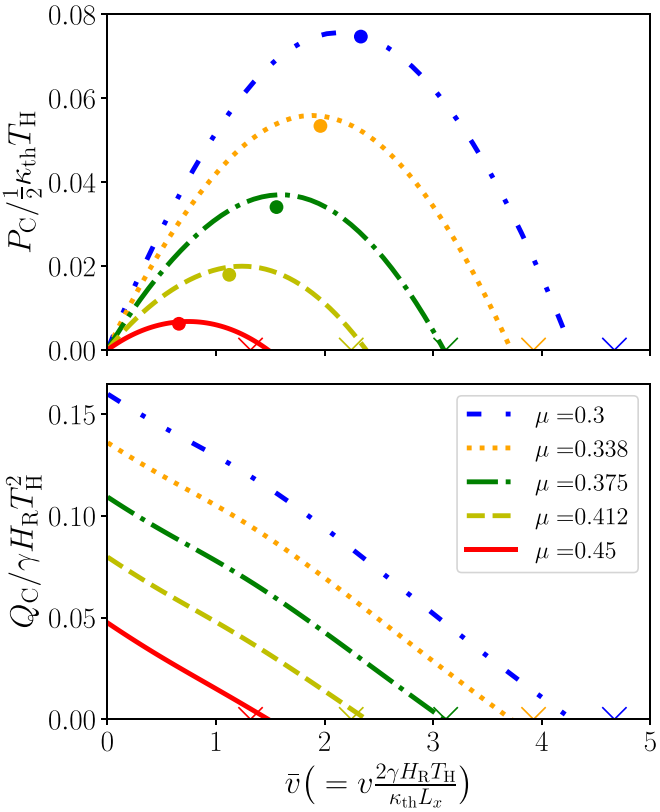

FIG. 5. Plot of scaled cooling power (top) and heat withdrawn from the cold reservoir (bottom) as functions of dimensionless fluxon velocity $\bar{v}$ for $l = 2.5$, $\Omega = 0.01$, $\phi_C = 0.5$ and different values of μ. The velocities v can be estimated (see Sec. IV B) to be of the order of 0.1 m/s. The dots in the top panel show the corresponding approximate cooling power maxima calculated analytically in Eq. (61). The crosses show Eq. (57), i.e., the velocity where both Q_C and P_C are 0. As μ decreases, the analytical approximations become worse at capturing the behavior. We can understand this by realizing that the $\mathcal{O}(\bar{v}^3)$ term in Eq. (59) has a coefficient proportional to $\phi_C - \mu^3$. Therefore, for the chosen parameter regime, as μ decreases, the higher-order effects become more prominent. Although not shown, the same effect can be observed as we increase the value of ϕ_C.

a reduced tunneling rate. However, we ignore such complications in the following calculations and provide an order of magnitude estimate. The above expression for small values of temperature difference $T - T_C \ll (T + T_C)/2$ evaluates to

$$P^{qp} \approx \frac{\pi^2 k_B^2 A}{3e^2 \mathcal{R}_s}(T_C - T)T_C. \tag{63}$$

Since the Fourier formula in Eq. (37) deals with unit volume heat transfer rate, comparing P^{qp} with $\dot{Q} \times wA$ leads to the expression for κ_{th},

$$\kappa_{th} = \frac{\pi^2 k_B^2 T_C}{3e^2 w \mathcal{R}_s}. \tag{64}$$

In general, κ_{th} can depend on the position of contact. We ignore the y dependence of κ_{th} for simplicity. Equivalently, the thermal conductivity in Eq. (64) can be assumed to be an average over the length of the arm (2). For numerical estimation, we look at the maximum cooling power predicted by expression (61)

$$P_{cooling} = P_C^{max} \times wA. \tag{65}$$

Now, assuming that the critical temperature of the superconductor is of the order of 10 K, we assume $T_H \sim T_C = 1K$. Additionally, we assume $A = 1mm^2$, $\mathcal{R}_s = 2M\omega m^2$[40,62], $\phi_C = 0.8$, $\mu = 0.5$, $l = 1$, $\Omega = 0.01$. Using Eqs. (61), (64), and (65) the maximum cooling power evaluates to be $P_{cooling} \sim$ nW (or equivalently nW/mm^2 of cooling power per unit area). Note that the specific resistance is chosen such that total resistance $\mathcal{R} = \mathcal{R}_s/A \sim 2\Omega$. For NIS junctions, specific resistance of the order of $10^3\ \Omega m^2$ can be fabricated [62], which can lead to a much higher cooling power. A microscopic description will require incorporation of junction properties as well as energy barrier experienced by fluxons going in and out of surface [63].

Next, we compute the speed of vortices moving in the Corbino geometry. From [54] we can write $\gamma = \frac{\gamma_n}{H_{c2}}$, and we assume an approximate value of $\gamma_n \sim 200\,\mathrm{J/m^3K^2}$. Additionally, we assume $\mu_0 H_{c2} = 50\,\mathrm{T}$ and $\mu_0 H_R = 1\,\mathrm{T}$ and a width of $w = 0.01\,\mathrm{mm}$. Now, from Fig. 5, we assume a dimensionless velocity $\bar{v} = 1$ and use Eqs. (51) and (64) to obtain $v \sim 0.1\,\mathrm{m/s}$, which is much smaller than Larkin-Ovchinnikov flux flow instability critical velocity [64] in typical, e.g., in Nb-based superconductors [65,66].

It is helpful to compare the estimated performance of our device to other refrigeration schemes based on quasiparticle tunneling, such as NIS junction refrigerators [6,60,67,68]. They are traditionally steady state refrigerators, where cooling is achieved by a voltage bias that drives hot electrons from a normal metal to a superconductor, against a temperature gradient. The quasiparticle current across the junction is usually suppressed due to the energy gap in the superconductor; however, the voltage bias supplies the necessary energy for hot electrons from the normal lead to overcome the superconducting gap energy.

In comparison, our cooling principle uses adiabatic magnetization. It lowers the temperature of the working fluxons to extract heat from the cold reservoir through quasiparticle tunneling into the fluxons, which are effectively puddles of normal regions. For otherwise identical parameters such as tunnel resistance, a normal/insulator/normal junction is more conductive than a superconducting/insulator/normal junction. Also, the scaling of cooling power with respect to temperature for NIS junction refrigerator is $T_e^{3/2}$ [67,68], while for and NIN junction it is T_e^2. Above T_e refers to the temperature of electrons.

C. Coefficient of performance

With insights on the fluxon temperatures throughout the cycle and cooling power, we are now in a position to characterize the refrigerator's performance. To compute the coefficient of performance using the dimensionless parameters, we can write Eq. (50) as

$$\begin{aligned} Q_H &= \gamma H_R T_H^2 \mu\left(l\bar{v}\Omega - \left(\tilde{\phi}_H^2 - \phi_L^2\right)\right), \\ &= \frac{Q_C}{\mu} + \gamma H_R T_H^2 \bar{v}\Omega\left[l(\mu + 1/\mu) + \frac{4}{3\mu}(1 + \mu + \mu^2)\right]. \end{aligned} \tag{66}$$

The total work done $W = Q_{\rm H} - Q_{\rm C}$

$$= \gamma H_{\rm R} T_{\rm H}^2 \big(l\bar{v}\Omega(1+\mu) - \mu(\tilde{\phi}_{\rm H}^2 - \phi_{\rm L}^2) - \big(\tilde{\phi}_{\rm C}^2 - \phi_{\rm R}^2\big)\big). \quad (67)$$

Here, the first term corresponds to the work done by the battery to maintain the electrical current. The rest of the terms express the work done to move the fluxons along the magnetic field gradient. Interestingly, the temperatures satisfy

$$\phi_{\rm L}^2 + \tilde{\phi}_{\rm H}^2 = \tfrac{1}{\mu^2}\big(\phi_{\rm R}^2 + \tilde{\phi}_{\rm C}^2\big). \quad (68)$$

We can write

$$\frac{Q_{\rm H}}{Q_{\rm C}} = \frac{\mu\big(l\bar{v}\Omega - \big(\tilde{\phi}_{\rm H}^2 - \phi_{\rm L}^2\big)\big)}{-l\bar{v}\Omega + \big(\tilde{\phi}_{\rm C}^2 - \phi_{\rm R}^2\big)}. \quad (69)$$

Using Eq. (69) we can calculate the coefficient of performance as $\mathrm{COP} = \frac{1}{Q_{\rm H}/Q_{\rm C}-1}$.

An important figure of merit for the refrigerator in view of achievable cooling is its coefficient of performance when the power output is maximum. For small fluxon speed, the coefficient of performance at maximum power (i.e., $\bar{v} = \bar{v}_{lim,\rm R}/2$) turns out to be $\mathrm{COP}(\mathrm{P}_{\rm C}^{\rm max}) \simeq$

$$\frac{\mu\big(l + \frac{2}{3}(1+\mu+\mu^2)\big)}{\big(l + \frac{2}{3}(1+\mu+\mu^2)\big)(3-\mu) - l(1-\mu^2)}. \quad (70)$$

Also, for $\bar{v} \simeq \bar{v}_{\rm lim,R}$, we have $P_{\rm C} = 0$ and $Q_{\rm C} = 0$. From Eq. (67) it is clear that, $Q_{\rm H}$ is not necessarily 0, leading to the fact that $\mathrm{COP}(\bar{\rm v} = \bar{\rm v}_{\rm lim,R}) = 0$. Moreover, as $\bar{v} \to 0$, $P_{\rm C} \to 0$ and $Q_{\rm C}$ is at a maximum value shown in Eq. (58). The heat transferred to the hot reservoir attains the minimum value $Q_{\rm H}^{\rm min} = \gamma H_{\rm R} T_{\rm H}^2(\phi_{\rm C}^2 - \mu^2)/\mu$. This leads to a maximum coefficient of performance $\mathrm{COP}^{\rm max} = \frac{\mu}{1-\mu}$. The highest value it can achieve is the Carnot coefficient of performance $\frac{\phi_{\rm C}}{1-\phi_{\rm C}}$ as $\mu \to \phi_{\rm C}$ and the cooling power goes to 0.

We show the behavior of the coefficient of performance [calculated using Eq. (69)] as a function of the dimensionless parameters l, μ, $\phi_{\rm C}$, $\bar{v}$, and Ω in Fig. 6. From the plots, it is clear that the dissipation, understandably, causes a decrease in the coefficient of performance. For small lengths l, the fluxons do not get to interact with the cold reservoir for much time. Therefore, with increasing length, the heat withdrawn, and consequently, the coefficient of performance increases. However, as we keep increasing the length, $Q_{\rm C}$ reaches a limiting value but the work done by the current source keeps increasing. This decreases the coefficient of performance. This observation also explains the flattening of the curves with decreasing Ω since the work needed to keep the current flowing also decreases. We see a similar behavior of the coefficient of performance as a function of the magnetic field ratio. As seen in Fig. 3, the COP first rises as a function of μ. However, as μ nears $\phi_{\rm C}$, the cooling power and therefore the COP decreases. Next, as we increase $\phi_{\rm C}$, more heat can be exchanged with the cold reservoir, thus leading to an increase in the COP. As $\phi_{\rm C} \to 1$, for small $\bar{v}$, the COP tends to Eq. (16). Finally, it can be argued that with increasing speed, the work done by the current source increases, and the heat withdrawn from the cold reservoir decreases, causing a significant decrease in the coefficient of performance.

These insights allude to the fact that for a given Ω, $\phi_{\rm C}$, and $\bar{v}$, we can choose μ and l that maximize the COP. Figure 7

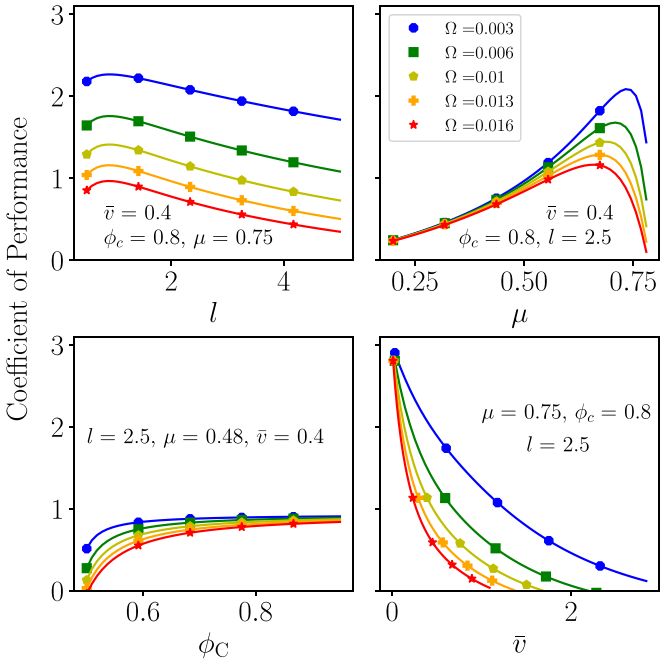

FIG. 6. Plots of the coefficient of performance as a function of l (top left), μ (top right), $\phi_{\rm C}$ (bottom left), and $\bar{v}$ (bottom right) for five different values of Ω. As one would anticipate, with decreasing dissipation (or Ω), the coefficient of performance increases. From the top left plot, we see that the COP first rises and then decreases as a function of length. We see a similar situation for the COP as a function of μ in the top right plot. As expected with refrigeration, we see in the bottom left plot that with increasing temperature ratio, the COP increases. It is worthwhile to mention that for the top two panels and the bottom right panel, the $\mathrm{COP}_{\rm Carnot}$ is 4.

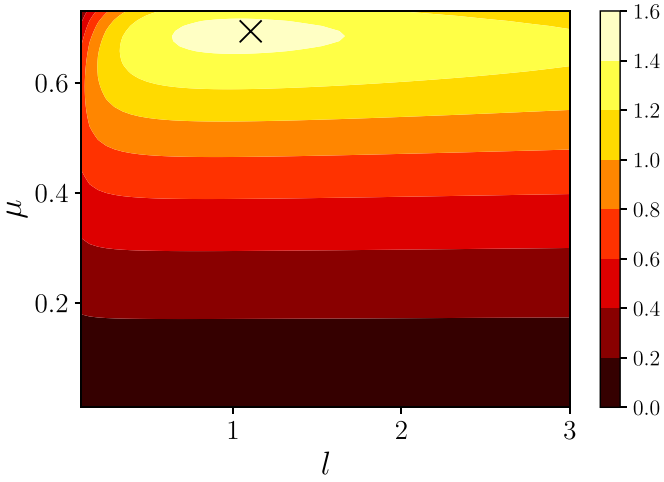

FIG. 7. Plot of the coefficient of performance as a function of μ and l, for $\phi_{\rm C} = 0.8$, $\bar{v} = 0.5$, and $\Omega = 0.01$. The brighter regions correspond to higher COP. The black "×" shows the maxima of the coefficient of performance calculated numerically. Due to dissipation, the maximum achievable COP (∼1.5) is less than $\mathrm{COP}_{\rm Carnot}$ (= 4), while the cooling power at the maximum COP is nonzero ($\sim 0.06\kappa_{\rm th}T_{\rm H}/2$).

shows the result of numerical maximization of the COP—or minimization of Eq. (69)—with respect to μ and l. Thus, for fixed bath temperatures, current and superconducting material, this analysis can be used to find an optimal value of the magnetic fields and the optimal geometry of the system.

V. DISCUSSION

Given that fluxons—which act like puddles of normal regions—predominantly carry the heat around the race-track cyclically, we considered a simple, Fourier law for heat transport across the interface for the steady state, where the heat current is proportional to the temperature difference across the interface, with the proportionality constant being the thermal conductivity of the interface. Such considerations, however, ignore different additional contributions to the heat transport possible in the system—originating from the energy level structure of the junction, or external voltage biases—and therefore have to be carefully accounted for to achieve the predicted cooling behavior in an experiment. For example, a small gap of the working superconductor can induce an above-the-gap quasiparticle transport from the hot to the cold reservoir across the sample, nullifying the cooling effect. Such quasiparticle transport across the working superconductor can be reduced by choosing either a superconductor of large gap as the working superconductor, or by biasing the chemical potential of the reservoirs below the gap energy of the working superconductor. In this regime, only subgap transfer of charge is possible, via Andreev reflections [69], as the quasiparticle heat transport becomes hindered by the energy gap of the working superconductor. Also, biasing the current source (which generates the circulation of fluxons) below the gap energy of the working superconductor further ensures that it will be a supercurrent (with no associated heat transfer) that generates the circulation, and not the above-the-gap quasiparticle current (which would add another heat contribution).

On a related note, superconductors with d-wave pairing symmetry have nodal directions where the gap energy goes to zero. Along these nodal directions, quasiparticle excitations can be present even at low temperatures (since they are no longer suppressed by the gap energy), and therefore can adversely affect the cooling process by inducing additional quasiparticle heat currents in the system.

Before we conclude, we wish to also comment on the role of phonons in the refrigeration process. The role of phonons is twofold for the systems considered here. Presently, we have assumed that quasielectrons and phonons decouple at low temperatures. The electron-phonon coupling scales as T^5, making their interaction very weak at low temperatures [6,70]. The cycles we describe are in the quasiequilibrium regime where the temperatures of the phonons and quasiparticles are different. As explained previously, along the adiabatic strokes, the density of states of the quasiparticles change. There is thermalization between the vortices due to quasiparticle exchange. At these low temperatures, we can ignore entropy exchanges between electrons and phonons in the transport of fluxons along the adiabatic arms of the cooling cycle. This results in simple linear cooling laws upon adiabatic magnetization, as we discussed here. On the other hand, when the interactions between quasielectrons and lattice phonons (which mediate superconductivity) occur much faster than the adiabatic timescale, we note that the cooperative effect of lattice-phonons can actually help improve the cooling effect. This can happen through a mechanism that is similar to adiabatic magnetization cooling of type-I superconductor [36,37,39,40]. When electron–lattice-phonon interactions are not negligible, the entropy that is preserved in adiabatic processes is the entropy of electrons plus the entropy of lattice-phonons. This results in a cubic advantage in cooling at low temperatures when electron–lattice-phonon interactions are not negligible. To see this, note that in the superconducting phase, electronic specific heat is negligible and the phononic contribution to entropy dominates, so $S_i \approx \alpha T_i^3$. In the final normal state realized by adiabatic magnetization; however, the electronic contribution to entropy dominates, therefore $S_f \approx \gamma(H_f)T_f$. Equating both assuming that the process is adiabatic, we find, $T_f = T_i^3/T_*^2$, where $T_* = \sqrt{\gamma(H_f)/\alpha}$. This effect could also be relevant for high-T_c, type-II superconductors, where one can operate the refrigerator cycles at higher temperatures. A microscopic description of the electron-phonon interaction can be interesting but is beyond the scope of our discussion.

The second aspect is the effect of phonon-phonon interactions across a given interface. Such interactions result in a heat transport between phonon-phonon interfaces i, j that is $\propto (T_{\mathrm{ph}_i}^4 - T_{\mathrm{ph}_j}^4)$ (known as the Kapitza coupling [71]). Although we have ignored the Kapitza coupling in our present paper, assuming phonon mismatch across the relevant interfaces, we note that it could become relevant, for example when cooling down a substrate of phonons in stacked architectures.

VI. CONCLUSIONS AND OUTLOOK

We presented a cyclic refrigerator using magnetic field vortices in a type-II superconductor as the working substance. This design joins other mesoscopic engines based on applied magnetic fields [7,40,72–74]. The thermodynamic cycle consists of two adiabatic steps and two isothermal steps, where the superconductor is in contact with thermal reservoirs in the latter parts of the cycle. For both s-wave and d-wave models, we describe the thermodynamic quantities associated with the refrigerator and calculate the corresponding coefficient of performance. We also discuss the limiting cases where the thermodynamically permissible maximum (Carnot) coefficient of performance is achieved, while the cooling power generically drops to zero as the transport becomes reversible. We show that the d-wave case, under otherwise identical conditions, leads to a higher coefficient of performance. We also characterize the heat flow dynamics from the superconductors to the reservoirs and provide a transitory description of the temperature of the fluxons. As we incorporate dissipation into our narrative, we notice a decrease in the coefficient of performance, as expected. Weak-pinning channels necessary for guided transport of fluxons we consider have been characterized experimentally in both linear [75,76] and circular geometries [77,78], and thus point at the near-term feasibility of experimental realizations of the refrigerators proposed here.

Our dynamical model dictates that the velocity of the fluxons (and therefore the applied current) has to be small enough to allow the fluxons to exchange heat with the reservoir during the isothermal steps. We also calculate the cooling power and show that it attains maxima for a certain value of the fluxon speed. Additionally, we show that, depending on system parameters and applied fields, there is an optimal geometry of the system that allows the highest coefficient of performance.

Our results point to several future ventures one could undertake. Presently, we looked at the steady-state dynamics of an ensemble of fluxons considering a mesoscopic sample. Their thermodynamics is well described by the fluxon gas limit as we discussed, and allows one to derive measurable figures of merit for the cyclic refrigerator, which can be tested in experiments. Beyond such explorations, it would also be exciting to explore the time-dependent, and transient behavior of the system considering a finite number of fluxons, as it might lead to insights on cyclic refrigeration in the small quantum systems' regime of thermodynamics, where fluctuations—including quantum fluctuations—also become relevant [79,80]; For example, making quantum mechanical observations of the dynamics of fluxons can incur a back-reaction on their dynamics, which could be harnessed to further improve the efficiencies of such microscopic devices [81–84]. We defer such analyses to future work.

ACKNOWLEDGMENTS

We gratefully acknowledge support from the U.S. Department of Energy (DOE), Office of Science, Basic Energy Sciences (BES), under Award No. DE-SC0017890. The work of S.K.M. was supported by the Wallenberg Initiative on Networks and Quantum Information (WINQ). Nordita is partially supported by Nordforsk. We also thank Francesco Giazotto, Britton Plourde, Matthew LaHaye, Alok Singh, Bibek Bhandari, and Sai Vijay Mocherla for helpful discussions.

APPENDIX: ALTERNATIVE ENTROPY GRADIENT CALCULATION FOR THE DISSIPATIVE CASE

In this section, we provide an alternative dynamic strategy of including energy dissipation into our consideration. For the adiabatic processes stroke 1 and 2, heat dissipated in time dt per unit volume at position x is $dQ = n(x)\eta v^2 dt$. Now, consider an element of length $dx = vdt$. Change in entropy of the fluxons due to dissipation $TdS = dQ$. In time dt, fluxons at x end up at $x + dx$. Therefore, if we express the unit volume entropy as a function of x and t,

$$S(x + dx, t + dt) = S(x, t) + \frac{n(x)\eta v}{T(x)} dx. \tag{A1}$$

This leads to

$$\frac{\partial S}{\partial x} + v\frac{\partial S}{\partial t} = \frac{n(x)\eta v}{T(x)}. \tag{A2}$$

For the steady state this reduces to

$$\frac{\partial S}{\partial x} = \frac{n(x)\eta v}{T(x)}, \tag{A3}$$

same as in Eq. (33).

[1] G. Benenti, G. Casati, K. Saito, and R. S. Whitney, Fundamental aspects of steady-state conversion of heat to work at the nanoscale, Phys. Rep. **694**, 1 (2017).
[2] B. Sothmann, R. Sánchez, and A. N. Jordan, Thermoelectric energy harvesting with quantum dots, Nanotechnology **26**, 032001 (2015).
[3] G. D. Mahan and J. O. Sofo, The best thermoelectric, Proc. Natl. Acad. Sci. USA **93**, 7436 (1996).
[4] H. van Houten, L. W. Molenkamp, C. W. J. Beenakker, and C. T. Foxon, Thermo-electric properties of quantum point contacts, Semicond. Sci. Technol. **7**, B215 (1992).
[5] A. N. Jordan, B. Sothmann, R. Sánchez, and M. Büttiker, Powerful and efficient energy harvester with resonant-tunneling quantum dots, Phys. Rev. B **87**, 075312 (2013).
[6] F. Giazotto, T. T. Heikkilä, A. Luukanen, A. M. Savin, and J. P. Pekola, Opportunities for mesoscopics in thermometry and refrigeration: Physics and applications, Rev. Mod. Phys. **78**, 217 (2006).
[7] R. Sánchez, B. Sothmann, and A. N. Jordan, Heat diode and engine based on quantum Hall edge states, New J. Phys. **17**, 075006 (2015).
[8] J. Yang, C. Elouard, J. Splettstoesser, B. Sothmann, R. Sánchez, and A. N. Jordan, Thermal transistor and thermometer based on Coulomb-coupled conductors, Phys. Rev. B **100**, 045418 (2019).
[9] S. K. Manikandan, É. Jussiau, and A. N. Jordan, Autonomous quantum absorption refrigerators, Phys. Rev. B **102**, 235427 (2020).
[10] R. Sánchez and M. Büttiker, Optimal energy quanta to current conversion, Phys. Rev. B **83**, 085428 (2011).
[11] B. Sothmann, R. Sánchez, A. N. Jordan, and M. Büttiker, Powerful energy harvester based on resonant-tunneling quantum wells, New J. Phys. **15**, 095021 (2013).
[12] B. Sothmann, R. Sánchez, A. N. Jordan, and M. Büttiker, Rectification of thermal fluctuations in a chaotic cavity heat engine, Phys. Rev. B **85**, 205301 (2012).
[13] Y. Choi and A. N. Jordan, Three-terminal heat engine and refrigerator based on superlattices, Physica E **74**, 465 (2015).
[14] B. Sothmann and M. Büttiker, Magnon-driven quantum-dot heat engine, Europhys. Lett. **99**, 27001 (2012).
[15] O.-P. Saira, M. Meschke, F. Giazotto, A. M. Savin, M. Möttönen, and J. P. Pekola, Heat transistor: Demonstration of gate-controlled electronic refrigeration, Phys. Rev. Lett. **99**, 027203 (2007).
[16] L. Henriet, A. N. Jordan, and K. Le Hur, Electrical current from quantum vacuum fluctuations in nanoengines, Phys. Rev. B **92**, 125306 (2015).
[17] P. P. Hofer, J.-R. Souquet, and A. A. Clerk, Quantum heat engine based on photon-assisted cooper pair tunneling, Phys. Rev. B **93**, 041418(R) (2016).

[18] J. R. Prance, C. G. Smith, J. P. Griffiths, S. J. Chorley, D. Anderson, G. A. C. Jones, I. Farrer, and D. A. Ritchie, Electronic refrigeration of a two-dimensional electron gas, Phys. Rev. Lett. **102**, 146602 (2009).

[19] G. Jaliel, R. K. Puddy, R. Sánchez, A. N. Jordan, B. Sothmann, I. Farrer, J. P. Griffiths, D. A. Ritchie, and C. G. Smith, Experimental realization of a quantum dot energy harvester, Phys. Rev. Lett. **123**, 117701 (2019).

[20] B. Roche, P. Roulleau, T. Jullien, Y. Jompol, I. Farrer, D. A. Ritchie, and D. C. Glattli, Harvesting dissipated energy with a mesoscopic ratchet, Nat. Commun. **6**, 6738 (2015).

[21] F. Hartmann, P. Pfeffer, S. Höfling, M. Kamp, and L. Worschech, Voltage fluctuation to current converter with Coulomb-coupled quantum dots, Phys. Rev. Lett. **114**, 146805 (2015).

[22] S. Dorsch, A. Svilans, M. Josefsson, B. Goldozian, M. Kumar, C. Thelander, A. Wacker, and A. Burke, Heat driven transport in serial double quantum dot devices, Nano Lett. **21**, 988 (2021).

[23] J. Senior, A. Gubaydullin, B. Karimi, J. T. Peltonen, J. Ankerhold, and J. P. Pekola, Heat rectification via a superconducting artificial atom, Commun. Phys. **3**, 40 (2020).

[24] A. Fornieri and F. Giazotto, Towards phase-coherent caloritronics in superconducting circuits, Nat. Nanotechnol. **12**, 944 (2017).

[25] H. Thierschmann, R. Sánchez, B. Sothmann, F. Arnold, C. Heyn, W. Hansen, H. Buhmann, and L. W. Molenkamp, Three-terminal energy harvester with coupled quantum dots, Nat. Nanotechnol. **10**, 854 (2015).

[26] M. Josefsson, A. Svilans, A. M. Burke, E. A. Hoffmann, S. Fahlvik, C. Thelander, M. Leijnse, and H. Linke, A quantum-dot heat engine operating close to the thermodynamic efficiency limits, Nat. Nanotechnol. **13**, 920 (2018).

[27] Z. B. Tan, A. Laitinen, N. S. Kirsanov, A. Galda, V. M. Vinokur, M. Haque, A. Savin, D. S. Golubev, G. B. Lesovik, and P. J. Hakonen, Thermoelectric current in a graphene cooper pair splitter, Nat. Commun. **12**, 138 (2021).

[28] A. A. Abrikosov, The magnetic properties of superconducting alloys, J. Phys. Chem. Solids **2**, 199 (1957).

[29] A. A. Abrikosov, Nobel lecture: Type-II superconductors and the vortex lattice, Rev. Mod. Phys. **76**, 975 (2004).

[30] M. Pioro-Ladriere, T. Obata, Y. Tokura, Y.-S. Shin, T. Kubo, K. Yoshida, T. Taniyama, and S. Tarucha, Electrically driven single-electron spin resonance in a slanting Zeeman field, Nat. Phys. **4**, 776 (2008).

[31] X. Wu, D. R. Ward, J. R. Prance, D. Kim, J. K. Gamble, R. T. Mohr, Z. Shi, D. E. Savage, M. G. Lagally, M. Friesen *et al.*, Two-axis control of a singlet–triplet qubit with an integrated micromagnet, Proc. Natl. Acad. Sci. U.S.A. **111**, 11938 (2014).

[32] H. Kim, L. Rózsa, D. Schreyer, E. Simon, and R. Wiesendanger, Long-range focusing of magnetic bound states in superconducting lanthanum, Nat. Commun. **11**, 4573 (2020).

[33] N. Banerjee, J. W. A. Robinson, and M. G. Blamire, Reversible control of spin-polarized supercurrents in ferromagnetic Josephson junctions, Nat. Commun. **5**, 4771 (2014).

[34] M. Tinkham, *Introduction to Superconductivity* (Dover Publications, Mineola, NY, 2004).

[35] L. Embon, Y. Anahory, Ž. L. Jelić, E. O. Lachman, Y. Myasoedov, M. E. Huber, G. P. Mikitik, A. V. Silhanek, M. V. Milošević, A. Gurevich *et al.*, Imaging of super-fast dynamics and flow instabilities of superconducting vortices, Nat. Commun. **8**, 85 (2017).

[36] W. H. Keesom and J. A. Kok, Further calorimetric experiments on thallium, Physica **1**, 595 (1934).

[37] K. Mendelssohn and J. R. Moore, Magneto-caloric effect in supraconducting tin, Nature (London) **133**, 413 (1934).

[38] M. Yaqub, Cooling by adiabatic magnetization of superconductors, Cryogenics **1**, 101 (1960).

[39] F. Dolcini and F. Giazotto, Adiabatic magnetization of superconductors as a high-performance cooling mechanism, Phys. Rev. B **80**, 024503 (2009).

[40] S. K. Manikandan, F. Giazotto, and A. N. Jordan, Superconducting quantum refrigerator: Breaking and rejoining cooper pairs with magnetic field cycles, Phys. Rev. Applied **11**, 054034 (2019).

[41] B. Rosenstein and D. Li, Ginzburg-Landau theory of type II superconductors in magnetic field, Rev. Mod. Phys. **82**, 109 (2010).

[42] T. Maniv, V. Zhuravlev, I. Vagner, and P. Wyder, Vortex states and quantum magnetic oscillations in conventional type-II superconductors, Rev. Mod. Phys. **73**, 867 (2001).

[43] J. E. Sonier, J. H. Brewer, and R. F. Kiefl, μ SR studies of the vortex state in type-II superconductors, Rev. Mod. Phys. **72**, 769 (2000).

[44] T. Golod, A. Iovan, and V. M. Krasnov, Single Abrikosov vortices as quantized information bits, Nat. Commun. **6**, 8628 (2015).

[45] O. V. Dobrovolskiy, R. Sachser, T. Brächer, T. Böttcher, V. V. Kruglyak, R. V. Vovk, V. A. Shklovskij, M. Huth, B. Hillebrands, and A. V. Chumak, Magnon–fluxon interaction in a ferromagnet/superconductor heterostructure, Nat. Phys. **15**, 477 (2019).

[46] C. Guarcello, F. Giazotto, and P. Solinas, Coherent diffraction of thermal currents in long Josephson tunnel junctions, Phys. Rev. B **94**, 054522 (2016).

[47] C. Guarcello, P. Solinas, A. Braggio, and F. Giazotto, Solitonic Josephson thermal transport, Phys. Rev. Appl. **9**, 034014 (2018).

[48] C. Guarcello, P. Solinas, A. Braggio, and F. Giazotto, Phase-coherent solitonic Josephson heat oscillator, Sci. Rep. **8**, 12287 (2018).

[49] C. Guarcello, P. Solinas, A. Braggio, and F. Giazotto, Solitonic thermal transport in a current-biased long Josephson junction, Phys. Rev. B **98**, 104501 (2018).

[50] C. Guarcello, P. Solinas, F. Giazotto, and A. Braggio, Thermal flux-flow regime in long Josephson tunnel junctions, J. Stat. Mech.: Theory Exp. **2019**, 084006 (2019).

[51] M. Mozurkewich and R. S. Berry, Optimal paths for thermodynamic systems: The ideal Otto cycle, J. Appl. Phys. **53**, 34 (1982).

[52] R. Kosloff and Y. Rezek, The quantum harmonic Otto cycle, Entropy **19**, 136 (2017).

[53] N. Lior and G. J. Rudy, Second-law analysis of an ideal Otto cycle, Energy Conversion and Management **28**, 327 (1988).

[54] H.-H. Wen, Specific heat in superconductors, Chin. Phys. B **29**, 017401 (2020).

[55] P. Mangin and R. Kahn, *Superconductivity: An Introduction* (Springer, Cham, 2017).

[56] Hereafter, all thermodynamic quantities are considered per unit volume.

[57] The right-hand side of Eq. (15) is zero because it corresponds to the variation of entropy during a cycle.
[58] G. Volovik, Superconductivity with lines of gap nodes: Density of states in the vortex, JETP Lett. **58**, 469 (1993).
[59] T. P. Orlando, *Foundations of Applied Superconductivity* (Addison-Wesley, Reading, MA, 1991).
[60] J. P. Pekola and F. W. J. Hekking, Normal-metal-superconductor tunnel junction as a Brownian refrigerator, Phys. Rev. Lett. **98**, 210604 (2007).
[61] G. Haack and F. Giazotto, Efficient and tunable Aharonov-Bohm quantum heat engine, Phys. Rev. B **100**, 235442 (2019).
[62] J. N. Ullom, Physics and applications of NIS junctions, AIP Conf. Proc. **605**, 135 (2002).
[63] C. P. Bean and J. D. Livingston, Surface barrier in type-II superconductors, Phys. Rev. Lett. **12**, 14 (1964).
[64] A. I. Larkin and Yu. N. Ovchinnikov, Nonlinear conductivity of superconductors in the mixed state, Sov. Phys. JETP **41**, 960 (1975).
[65] D. Babić, J. Bentner, C. Sürgers, and C. Strunk, Flux-flow instabilities in amorphous $Nb_{0.7}Ge_{0.3}$ microbridges, Phys. Rev. B **69**, 092510 (2004).
[66] A. I. Bezuglyj, V. A. Shklovskij, R. V. Vovk, V. M. Bevz, M. Huth, and O. V. Dobrovolskiy, Local flux-flow instability in superconducting films near T_c, Phys. Rev. B **99**, 174518 (2019).
[67] H. Courtois, H. Q. Nguyen, C. B. Winkelmann, and J. P. Pekola, High-performance electronic cooling with superconducting tunnel junctions, C. R. Phys. **17**, 1139 (2016).
[68] J. P. Pekola, J. M. Kyynäräinen, M. M. Leivo, and A. J. Manninen, NIS chip refrigeration, Cryogenics **39**, 653 (1999).
[69] A. F. Andreev, Thermal conductivity of the intermediate state of superconductors, Zh. Eksperim. i Teor. Fiz. **46**, 1823 (1964).
[70] J. T. Muhonen, M. Meschke, and J. P. Pekola, Micrometre-scale refrigerators, Rep. Prog. Phys. **75**, 046501 (2012).
[71] G. L. Pollack, Kapitza resistance, Rev. Mod. Phys. **41**, 48 (1969).
[72] J. Atalaya and L. Y. Gorelik, Spintronics-based mesoscopic heat engine, Phys. Rev. B **85**, 245309 (2012).
[73] B. Sothmann, R. Sánchez, and A. N. Jordan, Quantum Nernst engines, Europhys. Lett. **107**, 47003 (2014).
[74] R. Sánchez, B. Sothmann, and A. N. Jordan, Chiral thermoelectrics with quantum Hall edge states, Phys. Rev. Lett. **114**, 146801 (2015).
[75] K. Yu, M. B. S. Hesselberth, P. H. Kes, and B. L. T. Plourde, Vortex dynamics in superconducting channels with periodic constrictions, Phys. Rev. B **81**, 184503 (2010).
[76] K. Yu, T. W. Heitmann, C. Song, M. P. DeFeo, B. L. T. Plourde, M. B. S. Hesselberth, and P. H. Kes, Asymmetric weak-pinning superconducting channels: Vortex ratchets, Phys. Rev. B **76**, 220507(R) (2007).
[77] N. S. Lin, T. W. Heitmann, K. Yu, B. L. T. Plourde, and V. R. Misko, Rectification of vortex motion in a circular ratchet channel, Phys. Rev. B **84**, 144511 (2011).
[78] T. W. Heitmann, K. Yu, C. Song, M. P. DeFeo, B. L. T. Plourde, M. B. S. Hesselberth, and P. H. Kes, Picovoltmeter for probing vortex dynamics in a single weak-pinning Corbino channel, Rev. Sci. Instrum. **79**, 103906 (2008).
[79] S. Vinjanampathy and J. Anders, Quantum thermodynamics, Contemp. Phys. **57**, 545 (2016).
[80] R. Kosloff, Quantum thermodynamics: A dynamical viewpoint, Entropy **15**, 2100 (2013).
[81] B. Bhandari and A. N. Jordan, Continuous measurement boosted adiabatic quantum thermal machines, Phys. Rev. Res. **4**, 033103 (2022).
[82] L. Buffoni, A. Solfanelli, P. Verrucchi, A. Cuccoli, and M. Campisi, Quantum measurement cooling, Phys. Rev. Lett. **122**, 070603 (2019).
[83] C. Elouard and A. N. Jordan, Efficient quantum measurement engines, Phys. Rev. Lett. **120**, 260601 (2018).
[84] C. Elouard, D. A. Herrera-Martí, M. Clusel, and A. Auffèves, The role of quantum measurement in stochastic thermodynamics, npj Quantum Inf. **3**, 9 (2017).